The V_2O_3(0001) surface termination: phase equilibrium

A.J. Window[1], A. Hentz[1*], D.C. Sheppard[1], G.S. Parkinson[1†], H. Niehus[2‡], D. Ahlbehrendt[2], T.C.Q. Noakes[3], P. Bailey[3], D.P. Woodruff[1,4*]

[1] *Physics Department, University of Warwick, Coventry CV4 7AL, UK*

[2] *Humboldt-Universität zu Berlin, Institut für Physik, Newtonstr. 15, D-12489 Berlin, Germany*

[3] *STFC Daresbury Laboratory, Warrington WA4 4AD, UK*

[4] *Fritz-Haber-Institut der Max-Planck-Gesellschaft, Faradyweg 4-6, 14195 Berlin, Germany*

Abstract

Complementary but independent medium-energy and low-energy ion scattering studies of the (0001) surfaces of V_2O_3 films grown on Pd(111), Au(111) and Cu_3Au(100) reveal a reconstructed full O_3-layer termination creating a VO_2 surface trilayer. This structure is fully consistent with previous calculations based on thermodynamic equilibrium at the surface during growth, but contrasts with previous suggestions that the surface termination comprises a complete monolayer of vanadyl (V=O) species.

PACS: 68.35.B-; 68.47.Gh; 68.49.Sf

[*] Present address: Universidade Federal do Rio Grande do Sul, Instituto de Fisica, Avenida Bento Gonçalves 9500, 91501-970 Porto Alegre, RS, Brazil

[†] Present address: Institüt für Angewandte Physik, TU Wien, 1040 Wien, Austria

[‡] Also at: Divisão de Metrologia de Materiais (DIMAT), INMETRO, CEP 25250-020, Xerém, Duque de Caxias, RJ, Brazil

[*] Corresponding author. Email d.p.woodruff@warwick.ac.uk

Oxide surfaces in general, and those of vanadium oxides in particular, play a major role in practical heterogeneous catalysis [1], yet there have been very few quantitative experimental structure determinations. The (0001) faces of corundum-phase structures, notably V_2O_3, α-Al_2O_3, and Cr_2O_3, are particularly interesting because there are several distinctly different atomic layers at which the bulk structure might be terminated. One fundamental question that is particularly relevant to these materials is whether, in practice, a surface can be created that is truly in equilibrium with its surroundings under preparation conditions. Starting from a bulk crystal of the oxide one might anticipate that it may be difficult to overcome the kinetic barriers to achieve this equilibrium under conditions of temperature and oxygen partial pressure accessible to surface science experiments. Alternatively, epitaxial growth of the oxide on a suitable substrate, by deposition of metal vapour in the presence of a partial pressure of oxygen, may offer a better means of achieving this gas-solid equilibrium. Growth is intrinsically a non-equilibrium process, yet by using low metal deposition rates in an excess of oxygen gas, the kinetic barriers to achieving equilibrium may be much lower than those needed to modify an existing non-equilibrium surface. In fact, previous structural studies of the surface of bulk crystals of α-Al_2O_3 and Cr_2O_3, and of Cr_2O_3 produced by oxidation of metallic Cr, appear to be broadly consistent with the theoretically-predicted equilibrium structure. By contrast, spectroscopic, imaging, and chemical studies of the V_2O_3(0001) surface of epitaxial films grown *in situ* have been interpreted in terms of a non-equilibrium surface (e.g. [2, 3, 4, 5, 6]). Here we show that two independent quantitative experimental determinations of the structure of V_2O_3(0001), using distinctly different ion scattering methods, demonstrate that the structure *does* correspond to the equilibrium state predicted in density functional theory (DFT) calculations. We find this is true for the surfaces of V_2O_3 films grown under conditions that are both similar to, and distinctly different from, those used in the earlier explorations of these surfaces. We discuss how these apparently conflicting views of the surface may be reconciled.

Relative to the (0001) basal plane, the bulk structure of V_2O_3 comprises alternate buckled layers containing 2 metal atoms per unit mesh, and planar layers containing 3 oxygen atoms per unit mesh; this layer structure is denoted here as ….O_3VV'O_3VV'O_3VV'….. (Fig. 1). Three distinct stoichiometric terminations of this bulk structure can be envisaged, namely oxygen …VV'O_3, full-metal ….O_3VV', (both polar surfaces), and half-metal ….V'O_3V.

Vibrational spectroscopy [2, 3] indicates that vanadyl species, V=O, occur on the surface, and this has, together with scanning tunnelling microscopy images [4] and X-ray absorption spectroscopy [5], been interpreted as indicating that the stable structure is half-metal terminated but with O atoms atop all surface V atoms to produce a (1x1) vanadyl phase (Fig. 1). However, DFT calculations show [7, 8] that for typical preparation temperatures (~600-900 K), and partial pressure of oxygen (~10^{-7}-10^{-5} mbar), the equilibrium surface structure should actually be oxygen-terminated, possibly with partial coverage of V=O species on this surface (Fig. 2). This O_3 termination is found to be stabilised by a reconstruction in which the upper half-layer of V atoms in the second VV' layer move up into the outermost VV' layer to produce a …$VO_3VV''V'O_3$ structure. In this termination the outermost $O_3V_3O_3$ layers have the stoichiometry and local structure characteristic of VO_2. According to these DFT results, the (1x1) pure vanadyl termination, ….$V'O_3V$=O, is never the equilibrium structure, but is closest to equilibrium at oxygen chemical potential values beyond the left-hand edge of Fig. 2, far from those achievable experimentally. The only previously-published experimental structural study, using photoelectron diffraction, provided support for a half-metal termination, with or without vanadyl O atoms, but did not consider the possibility of the O_3 termination [9]. An unpublished low energy electron diffraction (LEED) study has found good theory-experiment agreement for the vanadyl-terminated structure [10].

The structural studies reported here exploit the techniques of medium-energy ion scattering (MEIS) and low-energy noble gas impact-collision ion scattering spectroscopy with detection of neutrals (NICISS) using, respectively, 100 keV H^+ and 3 keV He^+ incident ions. The MEIS experiments were performed at the Daresbury Laboratory UK National MEIS facility [11] on V_2O_3(0001) films grown *in situ* on Pd(111) and Au(111) substrates. The NICISS data, obtained in a true 180° backscattering geometry [12], were obtained at the Humboldt University in Berlin [13] on V_2O_3(0001) films grown on a Cu_3Au(100) substrate. Note that the fact that the symmetries of the substrates contain elements not present in V_2O_3 (mirror planes on fcc(111) surface, mirror planes and 4-fold rotation on fcc(100)) leads to multiple mirror and rotational domains with equal occupation in the oxide films. On Pd(111), films ~ 20 Å thickness were grown using a sequence of ~5 doses of ~10 mins V vapour deposition in an oxygen partial pressure of 2x10^{-7} mbar with a sample temperature of

~570 K, followed by heating to ~670 K for 1-2 mins in vacuum. On Au(111) films up to 200 Å thickness were grown using a single dose (1-3 hours) at the same temperature and partial pressure, followed by annealing for 10-20 mins at 770 K in an oxygen pressure of $5x10^{-8}$ mbar. Both methods are closely similar to those used previously by others [3, 4]. Growth on $Cu_3Au(100)$, oxygen pretreated to form a CAOS (Copper Au Oxygen Surface) substrate, was effected by depositing V at 300 K, followed by annealing at 650 K in $5x10^{-7}$ mbar oxygen, leading to a $V_2O_3(0001)$ film thickness of ~25 Å [13, 14].

Both ion scattering methods exploit the influence of 'shadow cones', created by elastic scattering from surface atoms, which exclude ions from regions behind the scattering atoms. In MEIS [15] (with narrow shadow cones ~0.2-0.3 Å) fixed incident geometries are chosen to illuminate a few near-surface atomic layers, and one exploits the shadow cones produced by the scattering from near-surface atoms that 'block' the outward trajectories of ions first scattered by atoms from lower atomic layers. Dips in the 'blocking curve' of scattered ion intensity as a function of scattering angle are thus characteristic of the relative positions of atoms in the outermost few atomic layers. In NICISS [12], using much lower energies, and He^+ rather than H^+ incident ions, the much stronger scattering and wider shadow cones (~2 Å) preclude significant sub-surface scattering. Using a 180° scattering angle, which ensures that shadowing effects are almost identical in incidence and scattered trajectories, one can exploit the near-neighbour shadowing of the outermost layer atoms. The NICISS experiments reported here were conducted at fixed grazing incidence angles and variable azimuthal angles.

Fig. 3 shows experimental MEIS blocking curves of scattering from V atoms, recorded at two different crystallographic incidence directions, compared with the results of simulations using the VEGAS computer code [16], for two different structural models. These experimental data were recorded from a 200 Å V_2O_3 film grown on Au(111); essentially identical data were obtained from the thinner films grown on Pd(111). Fig. 3 shows clearly that the simulations based on the vanadyl termination gives poor agreement with the experimental data, despite adjustments to the interlayer spacings to optimise the fits. A simple half-metal termination simulation yields very similar blocking curves. By contrast, the simulation for the reconstructed O_3 termination model gives good agreement with

experiment.

Fig. 4 shows the key experimental results of the NICISS experiments; azimuthal scans of the scattered ion yield from V atoms, recorded at two different grazing incidence angles, are compared with the results of simulations using the FAN computer code [17] for the same two structural models. For these data, too, the simulations based on the reconstructed O_3 termination model provide a greatly superior description of the experimental data. In particular, all the main maxima in the experimental azimuthal plots recorded at 11° incidence switch to main minima when the incidence angle is increased to 16°; this behaviour is reproduced for the O_3 termination, but not for the vanadyl model, nor for other models tested including half-metal and full-metal terminations (not shown). Table 1 provides a comparison of the best-fit values of the outermost interlayer spacings found in the two experimental studies and in the earlier DFT calculations; the agreement is good and the results are consistent.

This structural conclusion for V_2O_3(0001) contrasts with that of previous experimental investigations of other corundum-phase surface structures, α-Al_2O_3(0001) [18, 19] and Cr_2O_3(0001) [20, 21, 22, 23]. For α-Al_2O_3(0001) the half-metal termination is favoured by LEED [18] and surface X-ray diffraction (SXRD) [19] studies, as well as DFT studies [24]. For Cr_2O_3(0001) the original LEED study also favoured a half-metal termination [20], but later work indicated there may be fractional occupation of other sites [21, 22, 23]. The main conclusions of the DFT calculations [25] for the predicted equilibrium phases of the surfaces of V_2O_3(0001) and Cr_2O_3(0001) at different oxygen chemical potential values in the gas phase are summarised in Fig. 2. For values in the range -1 eV to -1.5 eV, typical of the preparation conditions, theory predicts for these two surfaces, the O_3 and half-metal terminations, respectively. Interestingly, at slightly smaller negative oxygen chemical potentials (higher partial pressures) the chromyl, Cr=O, termination becomes stable on Cr_2O_3, consistent with observation of the associated Cr-O stretching mode in vibrational spectroscopy after oxygen exposure [26]. These results are also broadly consistent with the results of the recent detailed SXRD study [23] which finds a chromyl termination at high oxygen pressures, although at lower pressures partial occupation of half-metal and full-metal sites is found. It appears, therefore, that with the exception of these full-metal sites, *all* these

surface studies of corundum-phase surfaces are consistent with the predicted thermodynamic equilibrium, whether produced from bulk crystals, oxidation of a metal crystal, or via epitaxial growth *in situ*. Note that Fig. 2 and this discussion relates to the equilibrium between the surface and gas phase; the DFT studies indicate that under most surface preparation conditions VO_2 and CrO_2 bulk phases are more stable that the V_2O_3 and Cr_2O_3, but these calculations take no account of the stabilising influence of the substrate epitaxy, nor of the energetic barrier to a bulk structural transformation.

It remains to account for previous conclusions that the $V_2O_3(0001)$ surface adopts the non-equilibrium (1x1) vanadyl termination. The observation of a vanadyl V=O stretching frequency in vibrational spectroscopy is the most significant evidence for this interpretation, this provides no information on the vanadyl coverage. In fact *partial* coverage of vanadyl species, on an otherwise reconstructed-O_3 termination, is consistent with the predicted equilibrium structure within a range of oxygen chemical potentials close to those experienced by the growing crystal (Fig. 2). Our results are not incompatible with this possibility, although we find no explicit evidence for their presence; while ion scattering simulations of (random) partial occupation of different sites cannot easily be performed, we estimate (from Figs. 3 and 4) that up to 10-20% partial occupation of vanadyl sites could be consistent with our data. A predominantly O_3 termination is also consistent with a photoelectron diffraction study of hydroxylated $V_2O_3(0001)$ which concluded that the hydroxylated O atoms occupied (predominantly or exclusively) sites in a complete O_3 layer, and not in surface vanadyl species [27]. STM might be expected to distinguish the vanadyl termination, with one V=O surface species per unit mesh, from the O_3 termination, with three surface O atoms per unit mesh, but theoretical simulations indicate that both terminations should lead to a single atomic-scale protrusion per unit mesh [28]. There seems good reason, therefore, to reassess the interpretation of some of the conclusions of earlier work on this surface insofar as they are be based on the assumption that the surface is fully vanadyl terminated. Our results indicate that is not the case, and that contrary to previous suggestions, the $V_2O_3(0001)$ surface structure, like that of $Cr_2O_3(0001)$ and α-$Al_2O_3(0001)$, does correspond to that predicted in DFT calculations of the thermodynamic equilibrium with the gas phase under preparation conditions. Specifically, $V_2O_3(0001)$ has a reconstructed O_3 termination, albeit with partial vanadyl coverage under some conditions.

Acknowledgements

The authors acknowledge the financial support of the Deutsche Forschungsgemeinschaft through the Sonderforschungsbereich 546 and the Engineering and Physical Sciences Research Council (UK). Veronica Ganduglia-Pirovano is thanked for valuable discussions.

Table 1. Interlayer spacings in the reconstructed O_3 model as found in the original DFT study [7] and in the MEIS and NICISS studies reported here. The labelling of the layers from the bulk is …V'(3)-O_3(3)-V(2)-O_3(2)-V(top)-V''(top)-V'(top)-O_3(top) . In NICISS ions do not penetrate to the sub-surface layers. The precision in the MEIS and NICISS values is ~±0.1 Å.

Parameter	DFT [7]	MEIS	NICISS
V'(top)-O_3(top) (Å)	0.86	0.91	0.85
V''(top)-V'(top) (Å)	0.19	0.18	0.05
V(top)-V''(top) (Å)	0.19	0.18	0.05
O_3(2)-V(top) (Å)	0.99	0.98	-
V(2)-O_3(2) (Å)	1.44	1.27	-
O_3(3)-V(2) (Å)	1.06	0.98	-
V'(3)-O_3(3) (Å)	(0.98)	1.07	-

Figure Captions

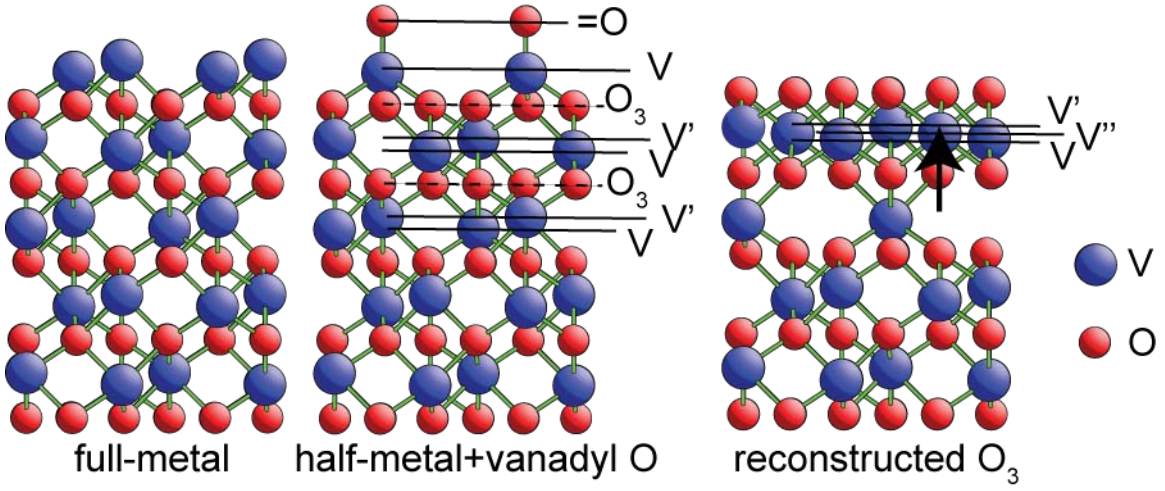

Fig. 1 Side views (viewed along $[2\bar{1}\bar{1}0]$) of $V_2O_3(0001)$, showing three possible surface terminations. In the reconstructed O_3 termination second-layer V' atoms move up to become V'' atoms in the outermost metal layer (see arrow).

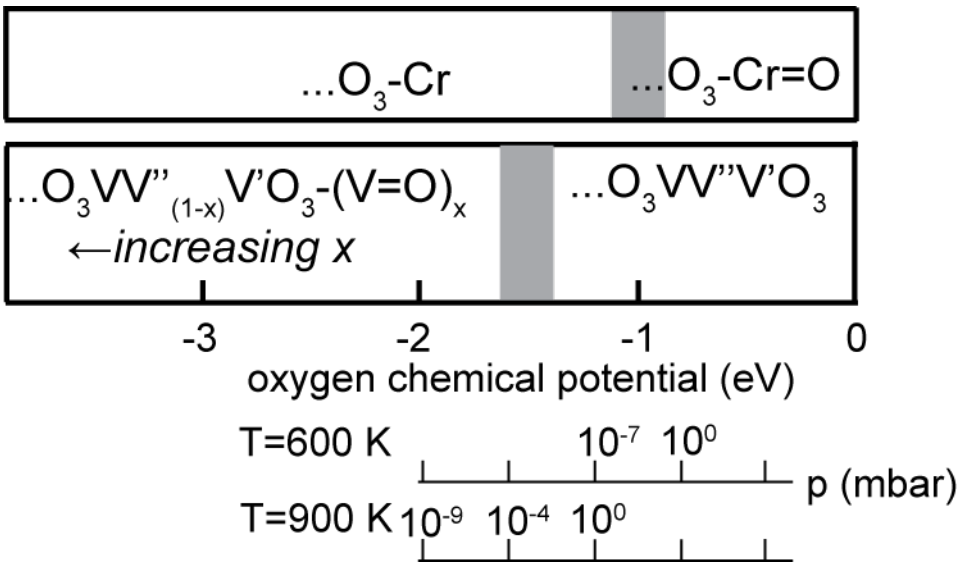

Fig. 2. Simplified diagram showing the equilibrium surface phases of the V_2O_3(0001) and Cr_2O_3(0001) surfaces under different conditions of oxygen partial pressure and temperature in DFT calculations [7, 25]. For V_2O_3 the region on the left corresponds to partial coverage of vanadyl V=O species; the calculations considered only two specific values of x, with x=1/3 corresponding to the chemical potential range ~-2.7 to -1.5 eV, and x=2/3 for larger (negative) values. The diffuse phase boundaries reflect some uncertainly in the associated chemical potential values, as reflected, for example, by different calculations for V_2O_3 [7, 8].

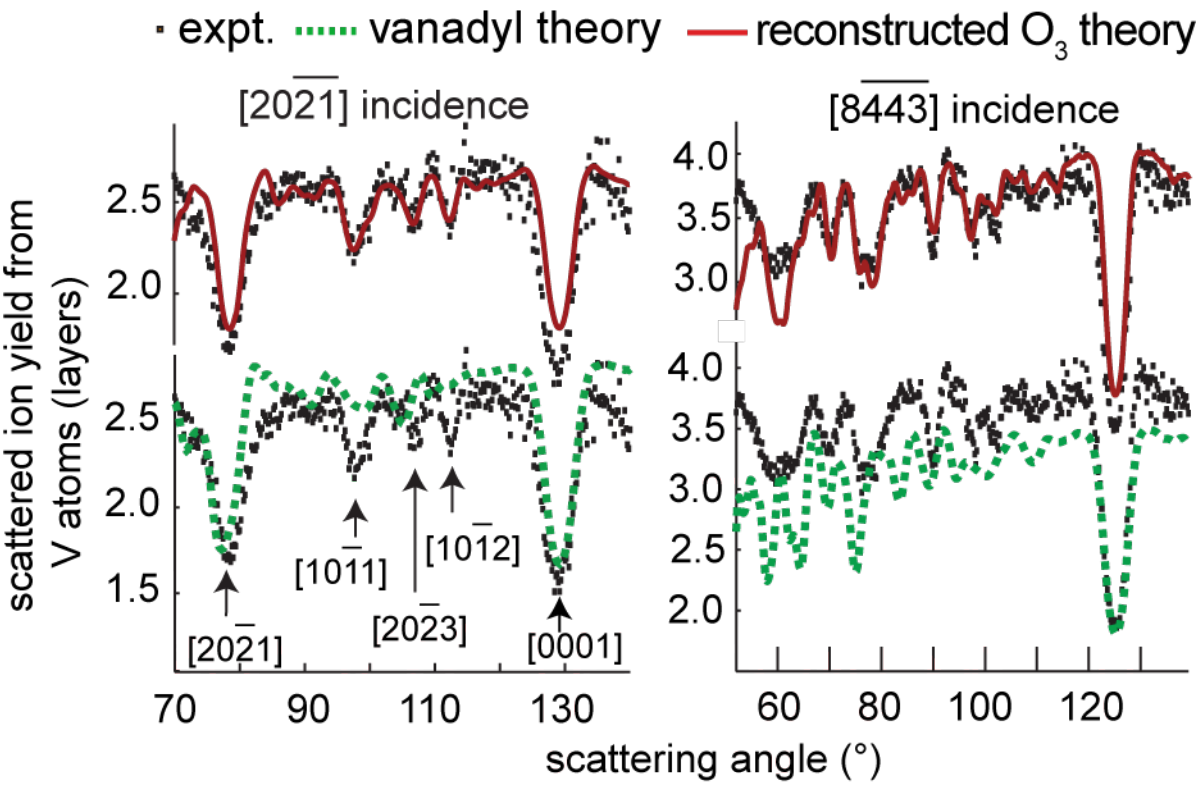

Fig. 3 Comparison of experimental 100 keV H^+ MEIS blocking curves from V_2O_3(0001) grown on Au(111), recorded in two different incidence directions, with the results of VEGAS simulations for the reconstructed O_3 and vanadyl termination models. The scattered ion yield is expressed in terms of the number of contributing atomic layers.

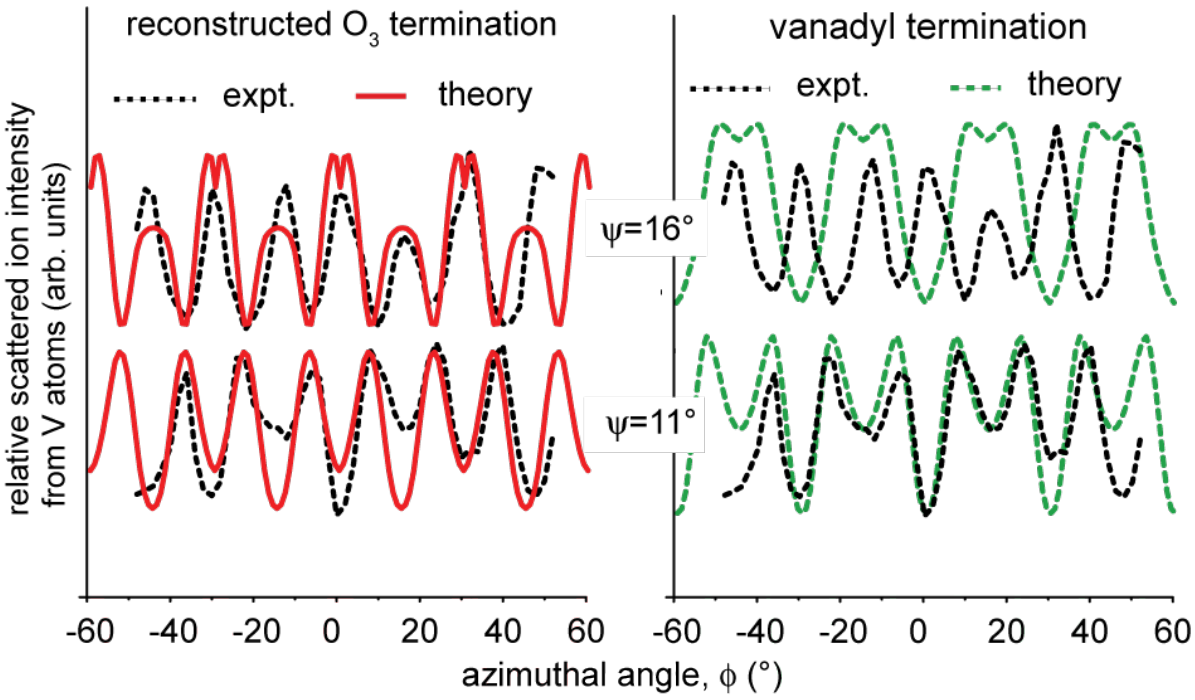

Fig. 4 Comparison of experimental 3 keV He^+ NICISS azimuthal scans from V_2O_3(0001) grown on Cu_3Au(100), recorded at two different grazing incidence angles, with the results of simulations for the reconstructed O_3, and the vanadyl termination models (Fig.1).

References

1 B. Grzybowska-Świerkosz, F. Trifirò, and J. C. Vedrine (eds) Appl. Catal. A **157**, 1 (1997).

2 J. Schoiswohl *et al.*, Surf. Sci. **555**, 101 (2004).

3 A. –C. Dupuis *et al.,* Surf. Sci. **539**, 99 (2003).

4 S. Surnev, M. G. Ramsey, and F. P. Netzer, Prog. Surf. Sci. **73**, 117 (2003).

5 C. Kolczewski *et al.,* Surface Sci. **601**, 5394 (2007).

6 D. Göbke *et al.,* Angew. Chem. Int. Ed. **48**, 3695 (2009).

7 G. Kresse *et al.,* Surf. Sci. **555**, 118 (2004).

8 T. K. Todorova, M. V. Ganduglia-Pirovano, and J. Sauer, J. Phys. Chem. **B 109**, 23523 (2005).

9 E. A. Kröger *et al.,* Surf. Sci. **601**, 3350 (2007).

10 Y. Romanyshyn and H. Kuhlenbeck, H. –J. Freund, to be published.

11 P. Bailey, T.C.Q. Noakes, and D.P. Woodruff, Surf. Sci. **426**, 358 (1999).

12 H. Niehus, W. Heiland, and E. Taglauer, Surf. Sci. Rep. **17**, 213 (1993)

13 H. Niehus, R. -P. Blum, and D. Ahlbehrendt, Surf. Rev. Lett., **10**, 353 (2003).

14 H. Niehus, R. P. Blum, and D. Ahlbehrendt, Phys. Stat. Sol. **A 187**, 151 (2001).

15 J.F. van der Veen, Surf. Sci. Rep. **5**, 199 (1985).

16 R.M. Tromp and J.F. van der Veen, Surf. Sci. **133**, 159 (1983).

17 H. Niehus and R. Spitzl, Surf. Interface Anal. **17**, 287 (1991); a free copy of the FAN code can be requested via e-mail to niehus@physik.hu-berlin.de

18 C.F. Walters *et al.*, Surf. Sci. **464**, L732 (2000).

19 P. Guénard *et al.,* Surf. Rev. Lett. **5**, 321 (1998).

20 R. Rohr *et al.,* Surf. Sci. **372**, L291 (1997); erratum **389**, 391 (1997).

21 Th. Gloege *et al.,* Surf. Sci. **441**, L917 (1999).

22 M. Lübbe and W. Moritz, J. Phys.: Condens. Matter **21**, 134010 (2009).

23 O. Bikondoa *et al.*, Ohys. Rev. B **81**, 205439 (2010).

24 R. Di Felice and J.E. Northrup, Phys. Rev. B **60**, 16287 (1999).

25 A. Rohrbach, J. Hafner, and G. Kresse, Phys. Rev. B **70**, 125426 (2004).

26 B. Dillmann *et al.,* Farad. Disc. **105**, 295 (1996).

27 E. A. Kröger *et al.,* Surf. Sci. **602**, 1267 (2008).

28 S. Surnev *et al.*, Surf. Sci. **495**, 91 (2001).